Pinning of a Bloch wall by diffusion of carbon atoms in a silicon-iron single crystal: an experimental study by means of an autoregressive spectrum analysis method

Nadine Martin, François Glangeaud, D. Guillet, Jean-Louis Porteseil

Short title : Pinning of a Bloch wall by diffusion of carbon atoms.

Classification number : 75-60 E

Abstract - Diffusion of intersticial carbon atoms in iron creates the phenomenon of "diffusion after-effect". After a recall of the main features of this effect, this paper reports on an experimental study of this phenomenon in a SiFe crystal. The various waveshapes generated by the motion of a single Bloch wall are analysed by an autoregressive signal processing technique which enables to study the "instantaneous" power spectrum. A simple model is proposed in order to account for the experimental results.

PINNING OF A BLOCH WALL BY DIFFUSION OF CARBON ATOMS IN A SILICON-IRON SINGLE CRYSTAL : AN EXPERIMENTAL STUDY BY MEANS OF AN AUTOREGRESSIVE SPECTRUM ANALYSIS METHOD.

N. MARTIN * , F. GLANGEAUD* , D. GUILLET ** and J.L. PORTESEIL **

* CEPHAG-ENSIEG, Domaine Universitaire, B.P. 46, 38402 Saint-Martin d'Hères, France.

** Laboratoire Louis Néel, CNRS-USMG, 166X, 38042 Grenoble-Cedex, France.

I - INTRODUCTION

Magnetisation processes in bulky materials are essentially due to motion of magnetic domain walls, at least in weak fields. In view of the number and intricacy of the phenomena involved, it is highly desirable to study the simplest possible domain structures. This paper reports a study of the motion of one 180° Bloch wall in a single crystal of Si-Fe, under conditions where diffusion of carbon atoms in the lattice interacts with the displacements of the wall.

2 - THE PHENOMENON OF "DIFFUSION AFTEREFFECT"

The mobility of domain walls is usually determined by lattice defects such as dislocations, inclusions, voids and vacancies ... However, in a magnetically soft material, another phenomenon, namely the diffusion after-effect, can become predominant in limited temperature ranges. This effect is associated with diffusion of impurity atoms inside a ferromagnetic material. Néel has given a detailed study of this phenomenon in the case of a solid solution of carbon atoms in the lattice of α-iron.

Fig.1 represents the body-centered unit cell of iron. The carbon atoms can be located in intersticial sites between two iron atoms along the X, Y or Z directions. If the symmetry of the lattice were perfectly cubic, the three possible types of sites would be rigorously equivalent. In fact, the spontaneous magnetization creates a dissymmetry between the X, Y and Z directions.

Néel argues that this dissymmetry can be taken into account by associating, to every intersticial site occupied by a carbon atom, an energy of the form $w \cos^2\phi$, where ϕ is the angle between the corresponding edge of the cube and the spontaneous magnetisation. This energy arises from the perturbation of magnetocrystalline couplings by the carbon atoms. Although an exact calculation of w would be an exceedingly difficult task, it can be estimated to lie in the range of 10^{-15} to 10^{-16} erg.

Consider now two adjacent domains in which the magnetisations are antiparallel. The magnetic moments rotate by 180° over a finite length which is the domain wall thickness : $\delta \simeq 2000$ Å in iron. If the wall is kept at rest for a very long time, thermal equilibrium is achieved by diffusion of carbon atoms. The proportions of occupied X, Y, and Z intersticial sites inside the wall are continuously varying functions of the Z coordinate and adjust themselves in order to decrease the energy of the system. Hence the wall traps itself in a potential well whose dimensions are of the order of δ .

The rate of creation of this well obviously depends on the time constant τ of diffusion of carbon atoms, which indeed is strongly temperature-dependent. This phenomenon was thoroughly studied by Brissonneau .

Suppose that the wall is constrained to move at a constant velocity $\dot{Z}$ by a suitable magnetic field. If the carbon atoms can diffuse at a sufficient rate, the potential well follows the wall in its motion across the crystal. Energy is then dissipated on a microscopic scale by reorientation of carbon atoms in the lattice, resulting in a damping force exerted on the wall.

This phenomenon can be assimilated to some kind of viscous friction (it should be stressed that the carbon atoms undergo a reorientation process, but no overall displacement of the cloud of intersticials is involved). On the other hand, if diffusion of carbon is too slow, the wall first jumps out of the potential well in which it was initially located, then moves on freely until it meets some obstacle or the magnetic field is decreased. This phenomenon was brought to evidence by Ferro et al .

The press The pressure exerted on the wall as a function of its velocity is given by the following relationship (Kronmüller, Grosse-Nobis and Shönfelder, Grosse-Nobis and Winner) :

$$p(\dot{Z}) = \frac{v_o}{\dot{Z}} \int_0^\infty \exp\left(-\frac{v_o}{\dot{Z}} \frac{Z}{\delta}\right) p_\infty (Z)dZ + \beta\dot{Z} \qquad (1)$$

where δ is the wall thickness ;

v_o is the characteristic velocity δ/τ ;

p_α (Z) is the pressure needed to displace by a distance Z the wall previously kept at rest for a time $t>>\tau$;

$\beta\dot{Z}$ represents the damping by macroscopic eddy currents.

Fig.2 is a sketch of the curve $p(\dot{Z})$. When $\dot{Z}$ is small with respect to δ/τ , the pressure is proportional to the velocity. The maximum of the curve corresponds to an infinitely high differential mobility and represents the possibility that the wall escapes the moving potential well. No stable motion can be obtained in the region of negative slope ; at very high velocities, the diffusion mechanism can be neglected, and the mobility is determined only by the eddy currents.

Cotillard et al. have studied the motion of a 180° Bloch wall and brought to evidence qualitative changes in the electromotive force generated by the wall as its velocity increases. We present hereafter a detailed study of this signal by suitable techniques of signal processing, and propose a model for the motion of the wall.

3 - THE SPECIMEN AND EXPERIMENTAL SETUP

The single crystal of SiFe contained 3% of silicon in weight. It was cut to the shape of a rectangular picture frame in a <001> plane, and its edges were parallel to the easy axes of the (100) type. The domain structure was determined by a mobile 180° wall running along the legs of the frame, and four fixed 90° walls in the corners (fig. 3).

The magnetic fields were applied by means of a primary coil wound around the four legs. A given displacement ΔZ of the 180° wall created, in a secondary coil, a change of magnetic flux $\Delta\phi \sim \Delta Z$. The magnetic fluxes were measured by means of an analog galvanometric fluxmeter (Vergne and Porteseil).

Since the material was a very soft one, even a slowly increasing field would have saturated it very rapidly, thus preventing any detailed study of the signal generated by the motion of the wall. We used the well-known technique (Mazzetti and Soardo) which consists of controlling the velocity of the wall by a feedback loop (fig. 4). A current proportional to the output voltage of the fluxmeter, that is to the flux change $\Delta\phi$, was fed to the magnetising coil with the suitable polarity. This feedback loop constrained the voltage ε at the input of the fluxmeter to be negligibly small. ε was the

algebraic sum of the induced voltage $-d\phi/dt$ and a reference e_r. Thus this setup enabled to impose a given rate of change of the magnetic flux, and consequently a given average velocity of the wall.

In the experiments reported hereafter, the temperature of the specimen was kept at 25± 0.1°C by a circulation of thermoregulated oil. At that temperature, the diffusion time constant of carbon atoms τ is close to one second ; accordingly, the characteristic velocity of the wall δ/τ was about 2000 $\mathring{A}.s^{-1}$, and the order of magnitude of the corresponding induced voltages, about 10^{-7}V, was well suited to the characteristics of the fluxmeter.

4 - EXPERIMENTAL RESULTS

We studied the behaviour of the 180° wall as a function of the reference velocity v_r, and observed that the voltage $-d\phi/dt$ induced in the secondary coil undergoes qualitative changes as v_r increases.

At very low velocities ($v_r < 100$ $\mathring{A}.s^{-1}$), the motion of the wall is essentially uniform, but for a very weak residual noise which can be attributed to the interaction with lattice defects. Increasing v_r leads to a quasi-periodic regime of voltage pulses : the wall moves by a succession of well-defined velocity jumps (fig. 5a). As v_r is further increased, the sequence of jumps becomes more and more complex (fig. 5 b,c) until it merges into a chaotic-looking regime (fig. 5 d).

The signals thus obtained for several values of v_r were adequately filtered in order to suppress the high-frequency noise and 50 Hz hum, then recorded on a magnetic tape.

Fig. 6 gives three typical examples of the waveshapes we studied.

5 - METHODS OF SIGNAL PROCESSING

We performed a preliminary study of the power spectra by means of a standard technique : correlation followed by a Fourier transform. That study yielded qualitatively correct results, especially that the power spectrum broadens as the signal evolves from the quasi-periodic regime to the chaotic one. However it turned out that the spectra were strongly dependent on the time interval over which they were determined. For that reason, we had to use more sophisticated signal-processing techniques providing information about the short-term characteristics of the signal.

5-1 - Moving-window Fourier transform

This technique consists of calculating the "instantaneous" power spectrum of the signal over a moving time window of finite duration T. It features two essential drawbacks : on the one hand, its frequency resolution becomes poor, of order 1/T, as the width of the window is decreased. On the other hand, it is not well suited to the study of a repetitive process which exhibits no long-term phase coherence.

5-2 - Autoregressive (AR) spectrum analysis

This parametric method allows to determine a finite number of frequencies, and was thoroughly described by Fargetton. In contrast with the classical techniques, its frequency resolution is no longer limiter by the duration of the signal,

thus allowing power spectra to be estimated over short time intervals. In that type of analysis, the signal is regarded as being the output of a filter whose parameters have to be determined by a suitable algorithm. Let x_n be the n^{th} sampled value of the signal x(t) ; the AR model of order M of the signal is defined by :

$$x_n = \sum_{i=1}^{M} a_i X_{n-i} + e_n \qquad (2)$$

with : a_i = coefficients of the model

$\sum_{i=1}^{M} a_i X_{n-i} = X_n$ value of x_n

predicted from the M previous values

$x_n - X_n = e_n$ error in the prediction of x_n

The AR algorithm enables to calculate the coefficient a_i by regarding e_n as a noise and minimising its power. The optimal method for estimating the a_i's is a least-square fit, which was especially designed to estimate evolutive power spectra : the algorithm adapts itself to the stationarity of the signal (Fargetton et al., Martin).

After having calculated the coefficients of the model, the power density is readily estimated as :

$$\gamma(\nu) = \frac{P_e t_e}{\left| 1 - \sum_{i=1}^{M} a_i \exp(-2\pi j \nu_i t_e) \right|^2} \qquad (3)$$

where T_e is the sampling period, and P_e the variance of the white noise e_n. This expression can also be written :

$$\gamma(Z) = \frac{P_e t_e}{\prod_{i}^{M} (Z - Z_i)}$$

The complex quantities Z_i, referred to as the poles of the AR model, are conveniently plotted in the complex plane inside the circle of radius 1 (fig. 7). Every pole represents a frequency existing in the signal ; the closer Z_i to the unit circle, the stronger the corresponding frequency.

6 - RESULTS OF THE FREQUENCY ANALYSIS

The results of these methods are compared hereafter for two different average velocities of the wall : 2040 and 2720 $\mathring{A}.s^{-1}$ (referred to as "low" and "medium" velocities). The sampling frequency was 4 Hz for both recordings ; the time window of the AR method was taken equal to 20 t_e = 5 s. The frequencies brought to evidence are plotted versus time on figs. 8 and 9. The solid lines represent the poles found by the AR method when their moduli are higher than 0.9, that is to say strong enough to represent unambiguously well-defined frequencies. On the other hand, the dotted contours represent the half-height widths of the peaks of the Fourier spectrum. The time windows of both methods are drawn at scale on fig. 9.

It can be seen from the figures that both types of analysis yield essentially the same kind of information ; especially, most of the solid segments (AR method) are located inside the dotted contours (Fourier transform). However, it turns out that the AR poles can be followed on time intervals during which the Fourier frequencies cannot be accurately defined.

The low-velocity recording exhibits a frequency fluctuating irregularly with time around 1 Hz. On the other hand, the medium-velocity recording brings to evidence two frequencies around 1 and 1.5 Hz, which seem to appear alternately. The way in which the instantaneous frequency shifts from one value to the other is illustrated by fig. 10. The upper part of the figure is a magnified plot of interval I (see fig. 9). The

solid lines represent, as previously, the main peaks of the Fourier spectrum, whereas the dotted lines represent weaker peak The corresponding waveshape is monitored on the lower part of figure 10 ; the "instantaneous" frequency clearly increases in the last quarter of the recording.

Fig. 11 gives three examples of the "instantaneous" power spectra determined by the AR method at three different times t_A, t_B, t_C (see fig. 9). It shows that, in the medium-speed regime, the two frequencies around 1 and 1.5 Hz coexist, but they do not have a high energy simultaneously. From these diagrams, it can be readily understood why the results of a standard Fourier analysis are strongly dependent on the time interval over which they are determined.

7 - A MODEL FOR THE MOTION OF THE WALL

We propose the following interpretation for the experimental results :

- When the reference velocity v_r is very low, the motion of the wall takes place on the region OA of the curve $p(\dot{z})$ (see fig. 2). In that region of positive slope $dp/d\dot{z}$, the motion is stable, that is to say a small variation of $\dot{z}$ tends to be cancelled by the corresponding change of the damping pressure.

- When v_r lies in the region of negative slope (AB), the motion is unstable. Suppose that the wall is initially at rest in 0 ; the velocity $\dot{z}$ first increases steadily towards its reference value up to v_A. Now, since the damping pressure decreases as $\dot{z}$ increases, the velocity jumps very rapidly up to v_C, where the stability is restored. Then the feedback loop decreases $\dot{z}$ in order to make it equal to v_r. When $\dot{z} = v_B$, the motion becomes unstable again, and another jump BD takes place, followed by a steady motion on the branch DA, and so on. Thus

the velocity cannot kept stable at its reference value. Such a mechanism results in a periodic motion (cycle ACBD), and may be invoked to explain the "low-velocity" quasi-periodic regime.

- The static lattice defects (essentially dislocations in our specimen) can account for the residual noise observed in region OA, and the fluctuation of the frequency around 1 Hz observed in the low-velocity recordings.

- The medium and high-velocity regimes (two frequencies and chaos) cannot be explained by a model in which the wall is regarded as a rigid plane. Hence one has to take into account some internal degrees of freedom of the wall. Of course, the lattice defects will also interact with that more complex kind of motion.

In the following, we will consider a unit area of the wall (1 cm^2).

7.1 - Motion of a rigid wall without lattice defects

The equation of motion is :

$$m\ddot{Z} + p(\dot{Z}) + f(Z,t) = 0 \qquad (4)$$

The mass m of the wall was taken equal to 1.4×10^{-10} $g.cm^{-2}$ (Chikazumi).

The term f(Z,t) stands for the pressure exerted on the wall by the feedback loop. The fluxmeter integrates the error voltage $e_r - (d\phi/dt)$ and feeds a force proportional to $\int(e_r - d\phi/dt)dt$ back to the wall. Since the changes of magnetic flux are proportional to the displacements of the wall, f(Z,t) can be written as $K(Z - v_r t)$; for our experimental setup, $K = 6.8 \times 10^3$ barye.cm^{-1}.

The damping pressure $p(\dot{Z})$ is given by equation (1), which is not well suited to a numerical study. In fact, its precise analytical form is unimportant ; the point is that the curve $p(\dot{Z})$ must exhibit a region of negative slope. After trying several analytical forms, we found that :

$$p(\dot{Z}) = K \frac{\dot{Z}/v_o}{1 + (\dot{Z}/v_o)^3} + \beta \dot{Z} \qquad (5)$$

is a satisfactory approximation to eq.(1) in the whole range of velocities. The numerical values of the parameters were determined as follows :

- $\beta = 0.542 \; M_S^2 \; \sigma \; d$, where σ and d stand for the conductivity and thickness of the specimen ; in our case $= 200$ baryes.s.cm^{-1} (Grosse-Nobis and Winner).

- From equation (5), the damping pressure originating from the diffusion after-effect passes through a maximum for $\dot{Z}/v_o = 0.79$. The corresponding value of $p(\dot{Z})$ is $P_{max} = 0.53$ K. We measured the field H_{max} applied by the feedback loop when a jump starts at point A (see fig.2) and found $H_{max} = 0.8$ mOe. Accordingly, $P_{max} = 2 M_S H_{max} = 2.7$ baryes, and K = 5.1 baryes.

Equation (1) was solved numerically. When v_r lies in the region of positive slope OA, the calculated velocity $\dot{Z}$ is always equal to v_r, but for a transient regime depending on the initial conditions. On the other hand, if v_r lies in the unstable region AB, a succession of periodic velocity pulses is obtained (fig. 12).

7.2. - Motion of a rigid wall with lattice defects

The lattice defects in the specimen exert on the wall a force $f_d(Z)$ which is a random fonction of its abscissa. That force can be regarded as the derivative of a suitable random potential V(Z). In Néel's model |14|, the curve V(Z) is assimilated to a succession of arcs of parabolas ; consequently, $f_d(Z)$ is made of a succession of linear segments, whose slopes are random. Porteseil et al. showed that the ends of these segments are separated by a distance of the order of the wall thickness δ . Accordingly, the random force due to defects was expressed in the internal $Z = n\delta$, $Z = (n+1)$ as :

$$f_d(Z) = - \frac{dV}{dZ} = p_n(Z-n\delta) + \text{constant} \qquad (6)$$

where p_n is the random slope on that interval, and the constant term is determined by imposing the continuity of $f_d(Z)$ et $Z = n\delta$

The simplest choice for the p_n's would be to consider them as independent random numbers. However, it turns out that these numbers are correlated over 5 or 6 successive segments of the curve $f_d(Z)$ (Porteseil et al.). A simple way of taking that memory into account consists of representing each p_n by the sum of 6 successive terms in a sequence of independent random numbers generated by a computer :

$$p_n = q_{n-5} + ... + q_n \qquad (7)$$

That process results in a correlation between p_n and p_m with decreases linearly with $|n-m|$ and vanishes when $|n-m| > 5$. The magnitude of the random slopes p_n was determined by imposing that the maximum value of the random force $f_d(Z)$ correspond to the experimental coercive field H_c of the specimen, which leads to $(f_d)_{max} = 9.5 \times 10^{-2}$ barye.

We solved numerically equation (4) in which the random term $f_d(Z)$ was added. Fig. 13 shows an example of the sequences of jumps thus generated. As could be expected, the amplitudes and time intervals are random ; nevertheless, the signal remains roughly periodic, like the experimental signal (fig. 5a). Fig.14 is an histogram of the time intervals between the jumps of the calculated sequence. It shows that a model of rigid wall with lattice defects can account for the quasi-periodic regime found experimentally at intermediate velocities.

7.3 - Model of two interacting pieces of wall with lattice defects

As previously stated, internal degrees of freedom have to be considered in order to describe the more complex (bi-periodic or chaotic) motion of the wall. We introduced them in the simplest possible way by assuming that the wall was made of two parts (fig. 15), each of them being subjected to a pressure whose analytical expression was analogous to equation (5). The two random contributions representing the influences of lattice defects on both parts were taken completely independent of each other. Furthermore, we introduced a restoring force of the type $M(Z_1-Z_2)$ in order to account for the increase of surface energy due to the distortion of the wall. From the currently admitted values of the wall energies in iron and iron alloys ($\gamma \simeq 1$ erg.cm^{-2}) we estimated $M \simeq 1$ dyne.cm^{-1}.

Then the problem consisted of solving numerically a system of two differential equations coupled by the spring-like interaction term M. Fig. 16 represents a calculated sequence of jumps. From the analysis of the results, it turns out that the wall may exhibit two different kinds of motion :

- a synchronous motion, in which both parts jump together ;
- a piecewise motion in which the parts of wall jump alternately.

Each kind of motion features a well defined average time interval between jumps which is shorter in the piecewise motion. For instance, with an average reference velocity of 10 000 $\mathring{A}.s^{-1}$, the average intervals are respectively about 0.4 and 0.24 s. Furthermore, it turns out that the motion shifts from one type to the other at random instants, depending on the values of the independent random forces exerted on both parts of the wall by the defects. This numerical study explains the main features of the bi-periodic regime observed at intermediate velocities, during which the repetition rate jumps from one value to another at random instants.

That analysis might indeed be extended to a higher number of segments of wall, in order to account for the chaotic-looking regime observed at high velocities. However that would not be very convincing, since a qualitative agreement with experiment could easily be achieved with a sufficient number of degrees of freedom, each of them being affected by a suitable random force. A more promising way consists of analysing the high-velocity signal by the "stroboscopic" technique widely used in the study of non-linear dynamical systems Dubois et al.). That technique would enable to determine experimentally the effective number of degrees of freedom, provided it is not too high, and perhaps to bring to evidence such characteristic structures as "strange attractors". That analysis is presently under way, and will be published elsewhere.

More generally, the motion of a domain wall is interesting because it enables to study the general behaviours encountered in non-linear dynamics in a situation typical of solid-state physics, where a "noise" due to defects is always present. For instance, the pinning of domain walls by diffusion of impurities might have some analogies with the pinning and memory effects observed in modulated structures and charge-density waves (Dumas et al., Lederer et al., Salva et al.).

Acknowledgments - The authors are indebted to P. Lorenzino for valuable help in performing the spectrum analyses.

REFERENCES

BRISSONNEAU P. 1957 Thesis (Univ.Grenoble)

CHIKAZUMI S. 1964 Physics of Magnetism, J. Wiley and Sons, Ed. (New York).

COTILLARD J.C., GUILLET D. and PORTESEIL J.L. 1982 Phys.Lett. A 88 219.

DUBOIS M., BERGE P. and CROQUETTE J. 1982 J.Physique Lettres 43, 295.

DUMAS J., ARBAOUI A., GUYOT H., MARCUS J. and SCHLENKER C., 1984 Phys.Rev.B 30, 2249.

FARGETTON H. 1979 Thesis (Univ.Grenoble)

FARGETTON H., GENDRIN R. and LACOUME J.L. 1980 Signal Processing Theories and Applications, Kunt M. and De Coulon F. Ed., North-Holland 777 to 792.

FERRO A., MAZZETTI P. and MONTALENTI G., 1965 Appl.Phys.Lett. 7, 118.

GROSSE-NOBIS W. and SCHÖNFELDER W., 1975 Physica B 80 , 407.

GROSSE-NOBIS W. and WINNER H., 1982 J.Mag.Mag.Mater. 26, 270.

KRONMÜLLER H. , 1968 Nachwirkung in Ferromagnetika, Springer Ed. (Berlin).

LEDERER P., MONTAMBAUX G., JAMET J.P. and CHAUVIN M., 1984 J.Physique Lettres 45, 627.

MARTIN N., 1984 Thesis (Univ.Grenoble)

MAZZETTI P. and SOARDO P., 1966 Rev.Sci.Instr., 37, 548

NEEL L. , 1942 Cahiers de Physique 12, 1.

NEEL L., 1952 J.Phys.Rad., 12, 249.

PORTESEIL J.L., VERGNE R. and COTILLARD J.C., 1977 J.Physique 38, 1541.

SALVA H., WANG Z.Z., MONCEAU P., RICHARD J. and RENARD H., 1984 Phil.Mag.B 49, 385.

VERGNE R. and PORTESEIL J.L., 1971 Rev.Phys.Appl . 6, 95.

FIGURE CAPTIONS

1 - The b.c.c cell of α-iron, showing the three possible types of carbon intersticials ; the Z site is occupied.

2 - A sketch of the damping pressure exerted on the wall as a function of its velocity.
For the clearness of the figure, the slope β of the asymptote (eddy currents) was strongly exaggerated. As a consequence, the velocity v_c indicated on the figure is much smaller than its actual order of magnitude. The insert shows the oscillations of the velocity when the reference velocity lies in the unstable region AB.

3 - The single crystal SiFe specimen. Outer dimensions : 37.20 x 17.26 mm^2 ; inter dimensions : 30.44 x 10.50 mm^2 ; thickness 0.61 mm.

4 - The feedback circuit enabling to control the velocity of the wall.

5 - Four examples of the signal generated in a pickup coil by the motion of the wall. Values of the references velocity v_r :
a : 1360 $\mathring{A}.s^{-1}$; b : 6800 $\mathring{A}.s^{-1}$; c : 10900 $\mathring{A}.s^{-1}$; d : 34000 $\mathring{A}.cm^-$
The length of the "t" arrow represents 5 s.

6 - Three examples of the waveshapes after low-pass filtering.

7 - The circle of radius 1 in the complex plane, showing the location of the poles of the AR method.

8 - Compared results of both types of frequency analysis for a reference velocity v_r = 2040 $\mathring{A}.s^{-1}$.

9 - Same as fig.8, v_r = 2720 $\mathring{A}.s^{-1}$.

10 - A detail of the waveshape and the corresponding change of the "instantaneous" frequency found by the AR method.

11 - Three examples of AR power spectra bringing to evidence the energy exchanges between two frequencies.

12 - The perfectly periodic velocity pulses obtained by solving numerically equation (4) with a reference velocity lying in the unstable region AB (see fig.2) : $v_r = 2040\ \mathring{A}.s^{-1}$.

13 - Same as fig. 12, with an additional random force representing the lattice defects.

14 - Histogram of the time intervals between jumps obtained from a long calculated sequence similar to fig. 13.

15 - A schematic model for the motion of a deformable wall made of two interacting parts.

16 - A sequence of velocity pulses calculated from the model of deformable wall interacting with lattice defects. The first six pulses correspond to the piecewise motion of the wall, the last four to its coherent motion.

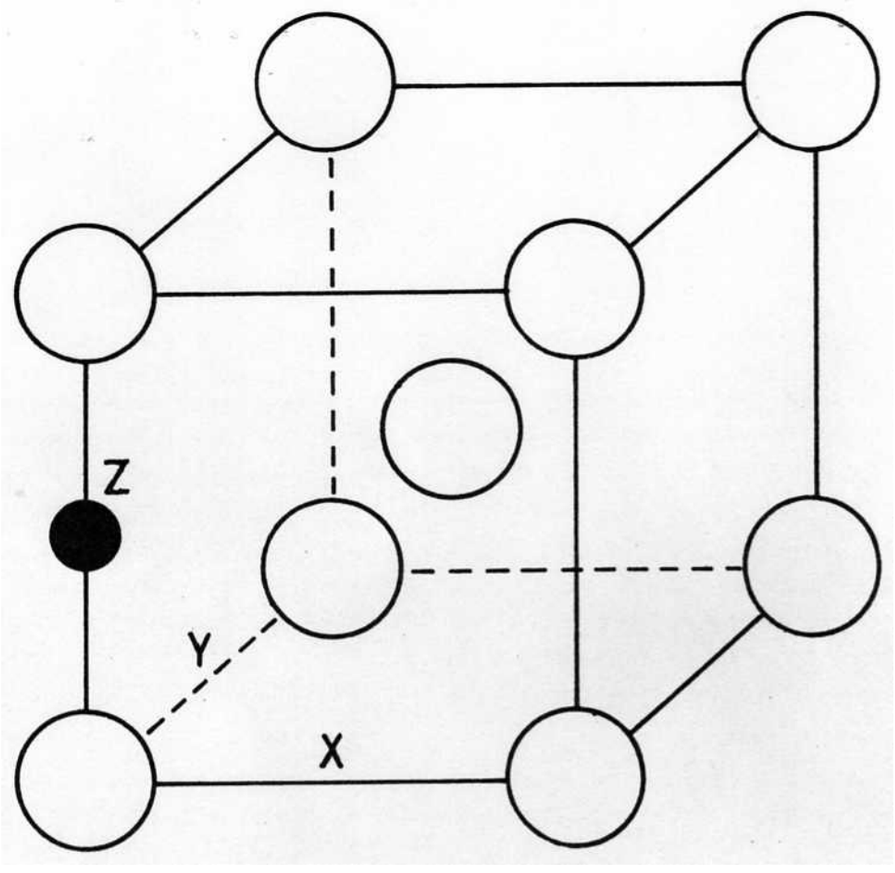
Z
Y
X

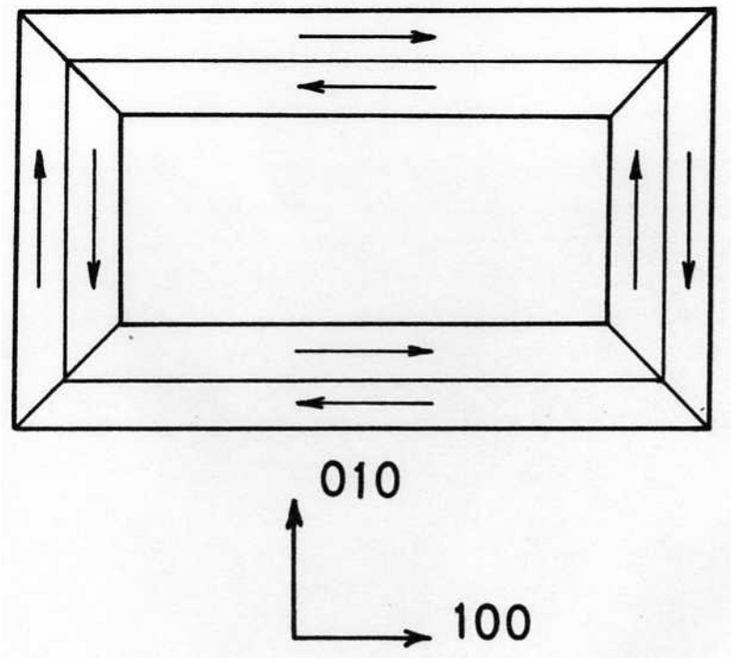
010
100

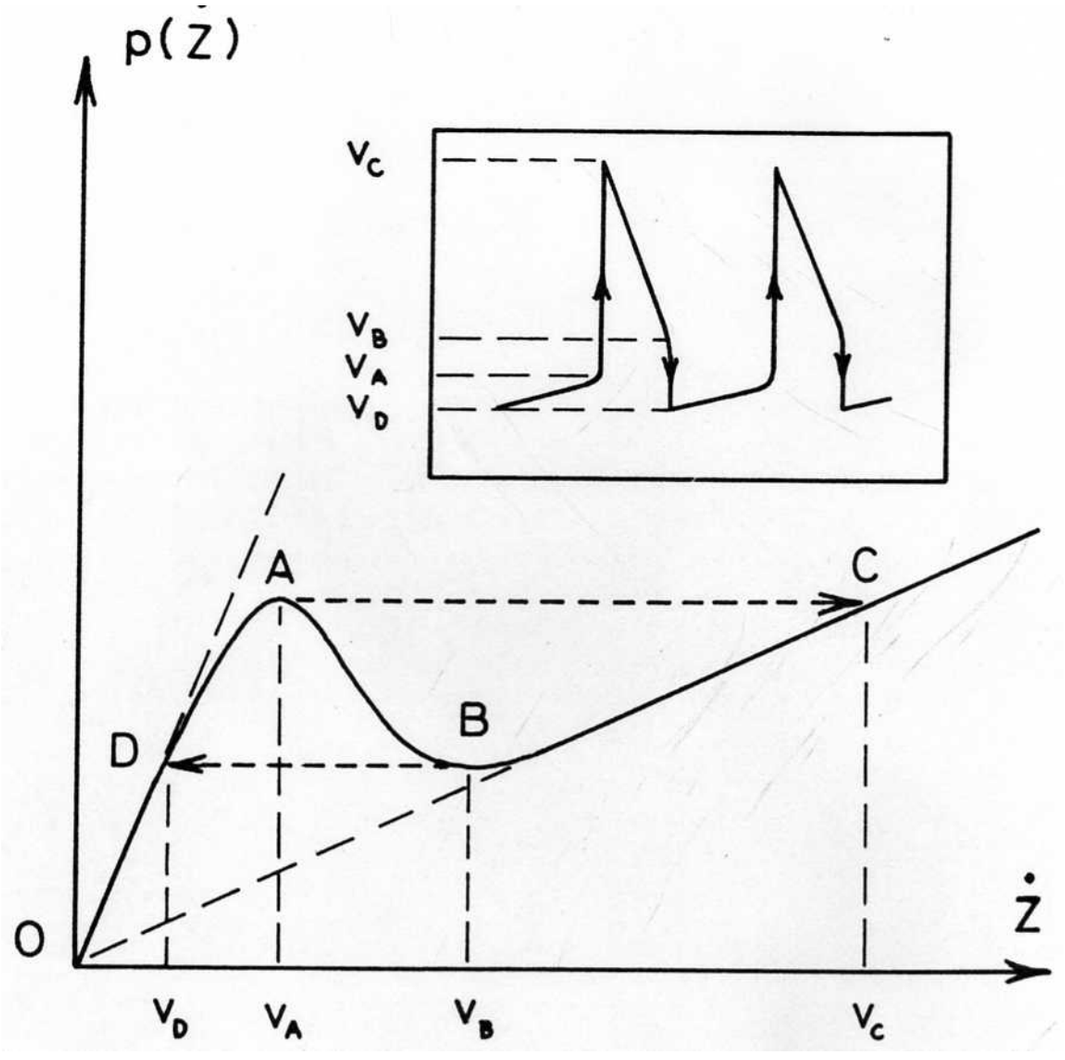
p(ż)
V_C
V_B
V_A
V_D
A
C
B
D
O
ż
V_D
V_A
V_B
V_C

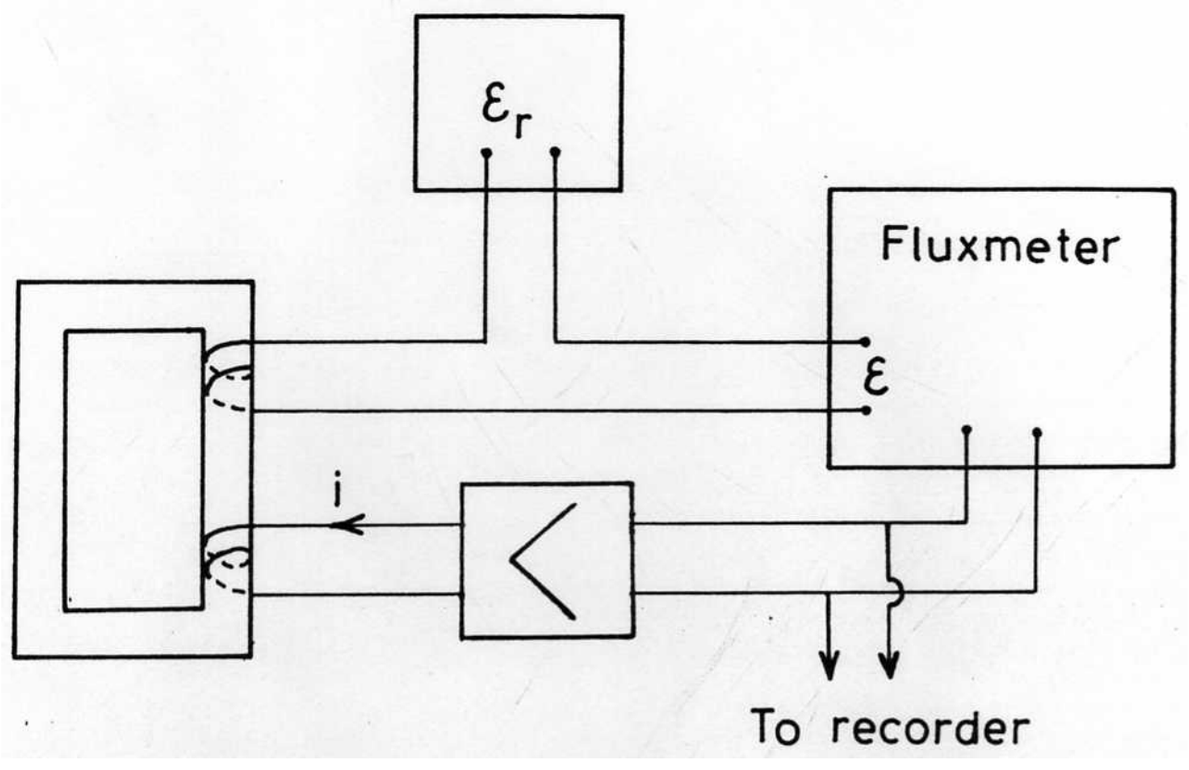
ε_r
Fluxmeter
ε
i
To recorder

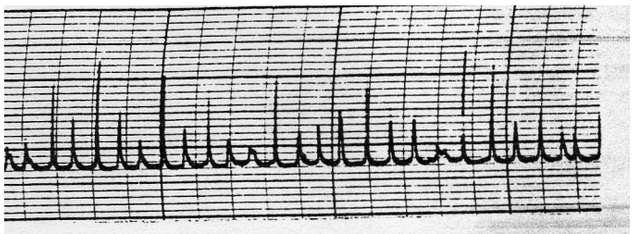

b

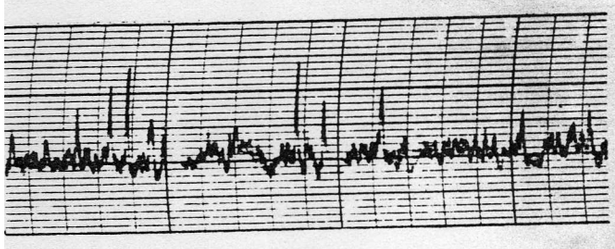

d

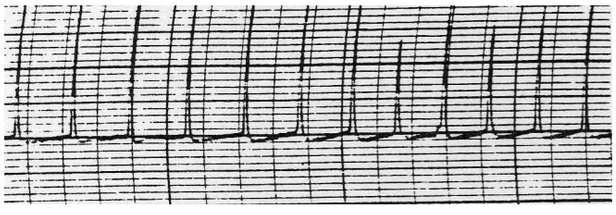

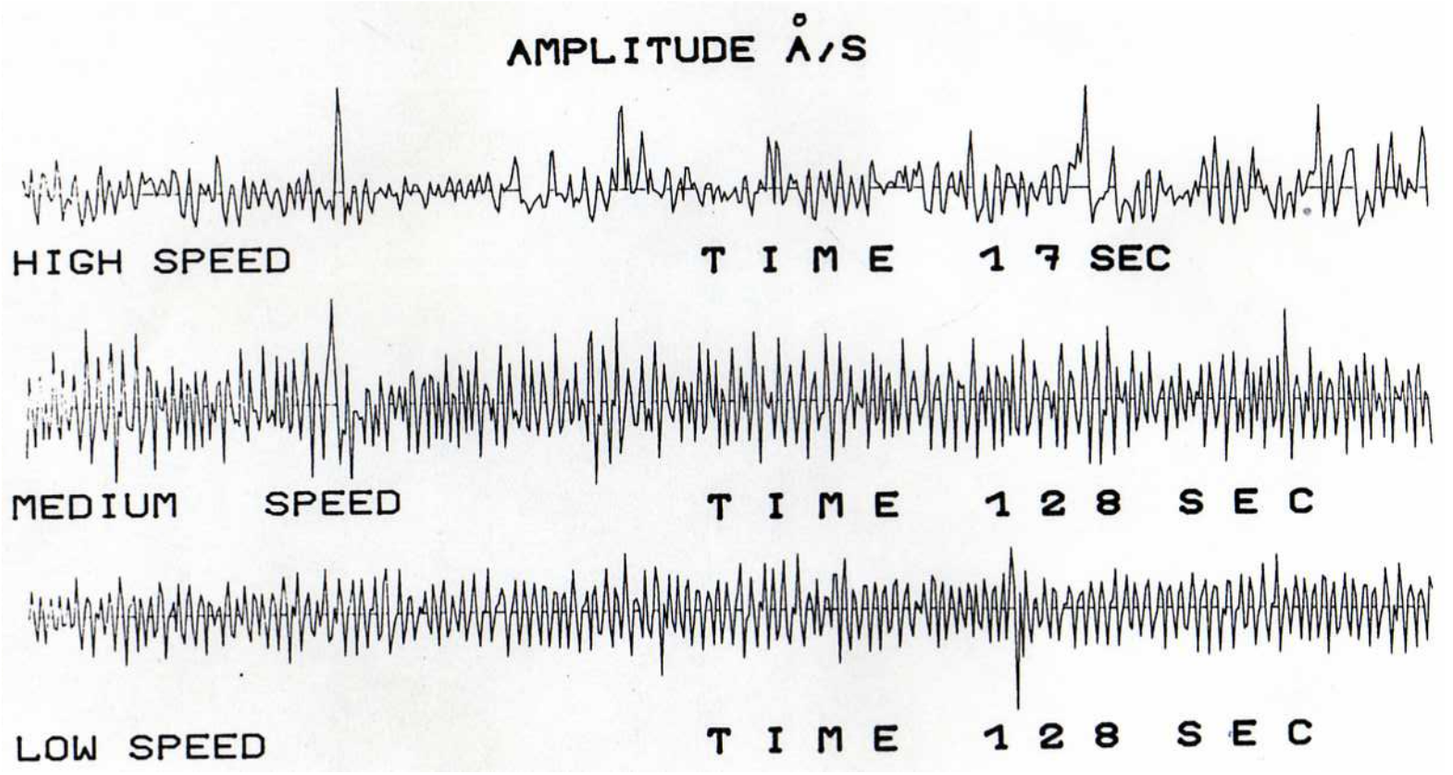
AMPLITUDE Å/S
HIGH SPEED
TIME 17 SEC
MEDIUM SPEED
TIME 128 SEC
LOW SPEED
TIME 128 SEC

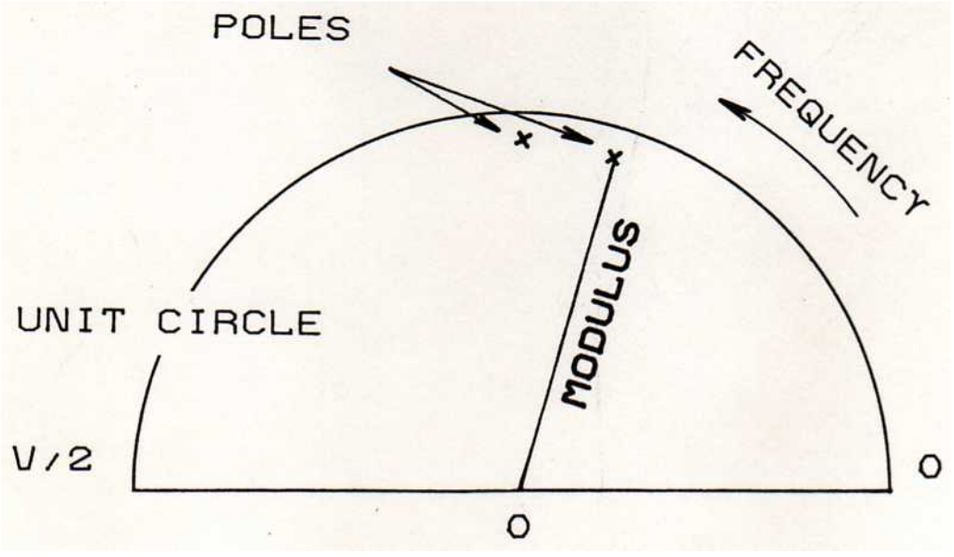
POLES
FREQUENCY
MODULUS
UNIT CIRCLE
V/2
0
0

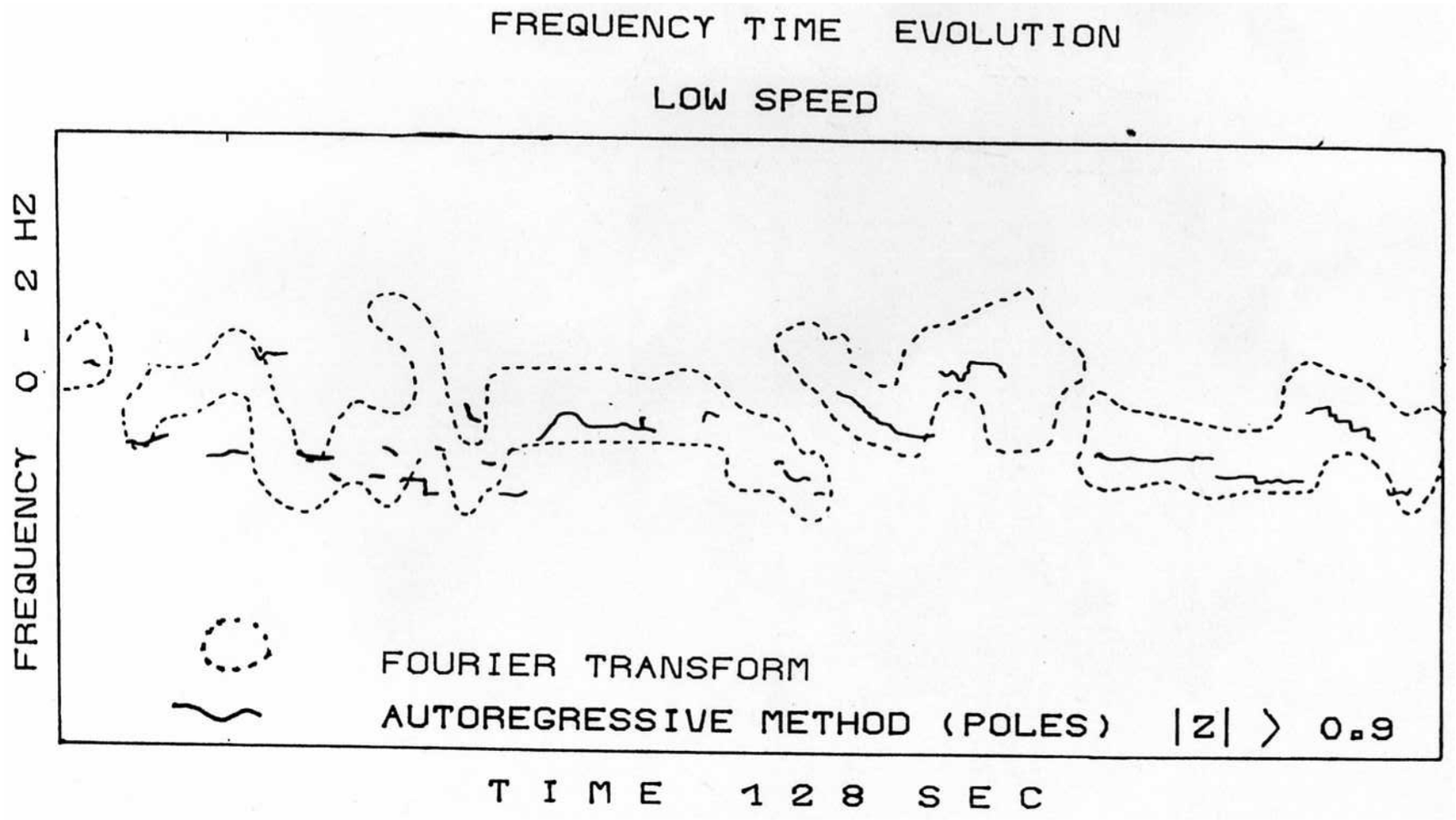
FREQUENCY TIME EVOLUTION
LOW SPEED
FREQUENCY 0 - 2 HZ
FOURIER TRANSFORM
AUTOREGRESSIVE METHOD (POLES) |Z| > 0.9
T I M E 1 2 8 S E C

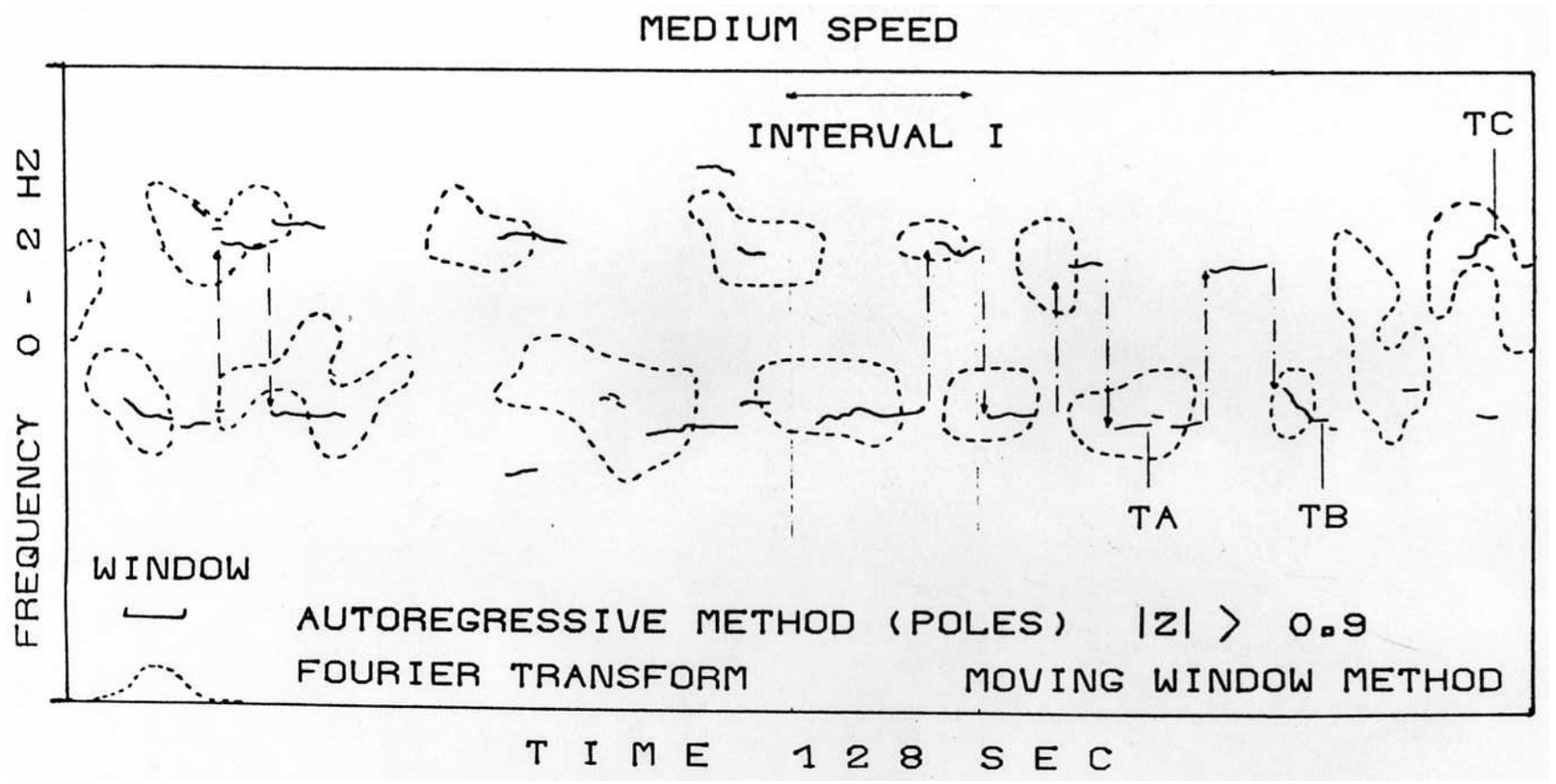
MEDIUM SPEED
INTERVAL I
TC
TA
TB
FREQUENCY 0 - 2 HZ
WINDOW
AUTOREGRESSIVE METHOD (POLES) |Z| > 0.9
FOURIER TRANSFORM
MOVING WINDOW METHOD
T I M E 1 2 8 S E C

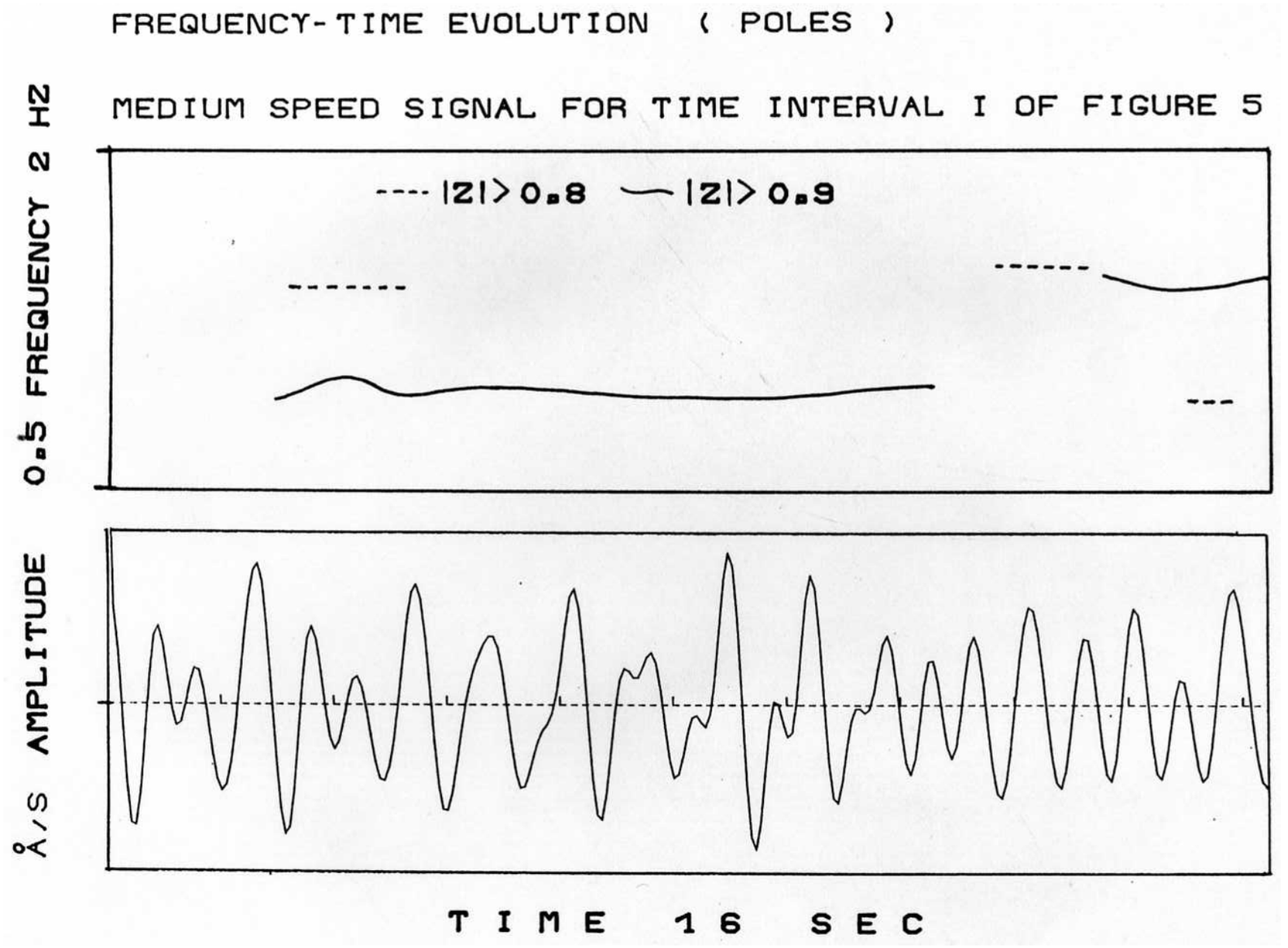
FREQUENCY-TIME EVOLUTION (POLES)
MEDIUM SPEED SIGNAL FOR TIME INTERVAL I OF FIGURE 5
0.5 FREQUENCY 2 HZ
---- |Z|> 0.8
— |Z|> 0.9
Å/S AMPLITUDE
TIME 16 SEC

POWER SPECTRAL DENSITY S AT THREE TIMES: TA, TB, TC (FIG 5)

PARAMETRIC METHOD (MEDIUM SPEED)

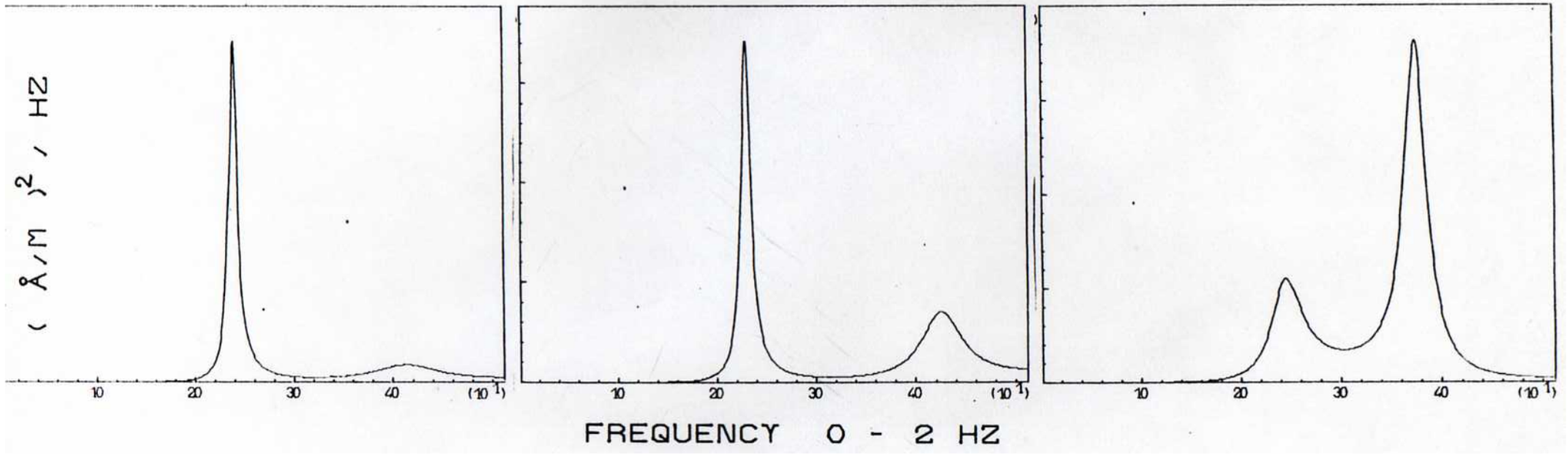

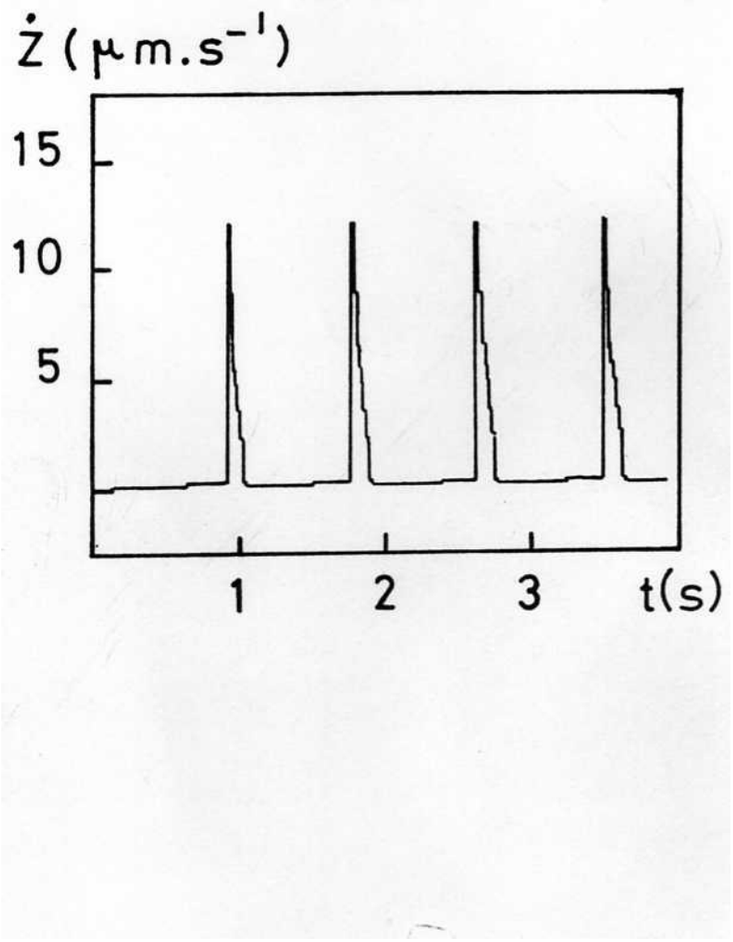
Ż (μm.s⁻¹)
15
10
5
1
2
3
t(s)

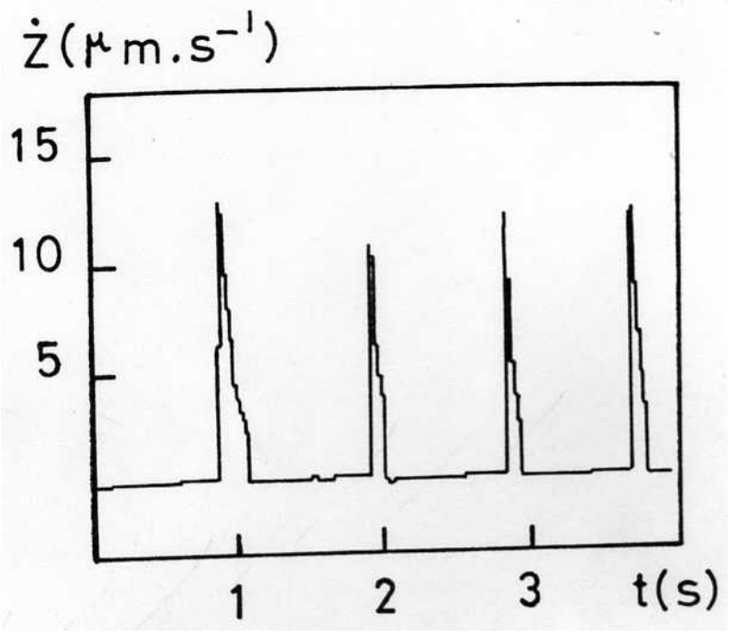
Ż(μm.s⁻¹)
15
10
5
1
2
3
t(s)

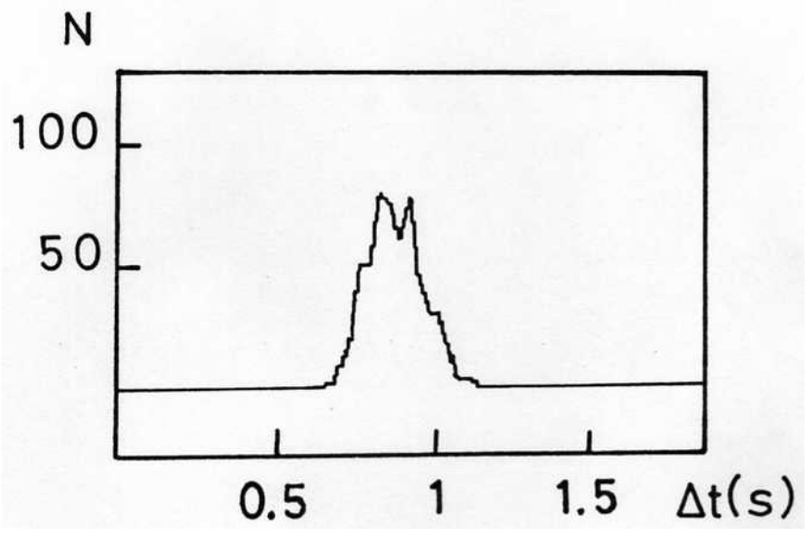
N
100
50
0.5
1
1.5
Δt(s)

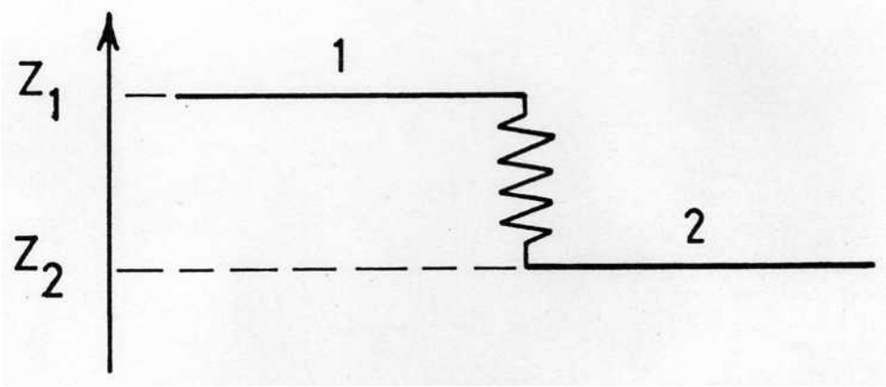
z_1
z_2
1
2

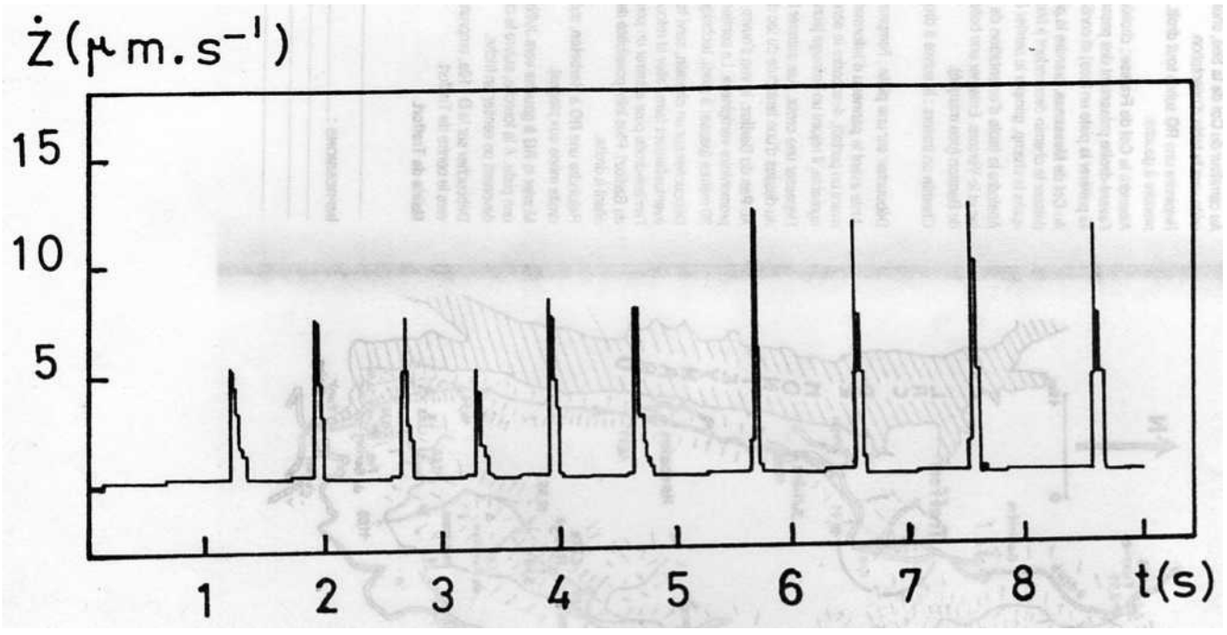
Ż(μm.s⁻¹)
15
10
5
1
2
3
4
5
6
7
8
t(s)